RESEARCH ARTICLE

Reciprocal regulation of actin cytoskeleton remodelling and cell migration by Ca²⁺ and Zn²⁺: role of TRPM2 channels

Fangfang Li[1,2], Nada Abuarab[1,2] and Asipu Sivaprasadarao[1,2,*]

ABSTRACT

Cell migration is a fundamental feature of tumour metastasis and angiogenesis. It is regulated by a variety of signalling molecules including H_2O_2 and Ca^{2+}. Here, we asked whether the H_2O_2-sensitive transient receptor potential melastatin 2 (TRPM2) Ca^{2+} channel serves as a molecular link between H_2O_2 and Ca^{2+}. H_2O_2-mediated activation of TRPM2 channels induced filopodia formation, loss of actin stress fibres and disassembly of focal adhesions, leading to increased migration of HeLa and prostate cancer (PC)-3 cells. Activation of TRPM2 channels, however, caused intracellular release of not only Ca^{2+} but also of Zn^{2+}. Intriguingly, elevation of intracellular Zn^{2+} faithfully reproduced all of the effects of H_2O_2, whereas Ca^{2+} showed opposite effects. Interestingly, H_2O_2 caused increased trafficking of Zn^{2+}-enriched lysosomes to the leading edge of migrating cells, presumably to impart polarisation of Zn^{2+} location. Thus, our results indicate that a reciprocal interplay between Ca^{2+} and Zn^{2+} regulates actin remodelling and cell migration; they call for a revision of the current notion that implicates an exclusive role for Ca^{2+} in cell migration.

KEY WORDS: Cell migration, TRPM2 channel, Actin cytoskeleton dynamics, Lysosomal trafficking, Focal adhesion, Ca^{2+}, Zn^{2+}

INTRODUCTION

Cell migration is a fundamental feature of angiogenesis (Lamalice et al., 2007), the leukocyte immune response (Klyubin et al., 1996) and tumour cell invasion (Ridley et al., 2003). It involves cyclical changes in cell morphology and focal adhesions that are spatiotemporally regulated. Changes in cell morphology are driven by the constant remodelling of the actin cytoskeleton into structures that coordinate cell migration (Gardel et al., 2010; Mattila and Lappalainen, 2008; Ridley et al., 2003; Small et al., 2002; Tojkander et al., 2012). These include filopodia (Mattila and Lappalainen, 2008), lamellipodia (Small et al., 2002) and stress fibres (Nobes and Hall, 1995; Tojkander et al., 2012). Filopodia are spike-like membrane projections where actin fibres assemble into tight bundles; they have the ability to sense motogenic signals (signals that direct cell migration) (Mattila and Lappalainen, 2008). Lamellipodia are brush-like protrusions formed at the leading edge of migrating cells, where actin polymerises into a cortical ring; they allow the front of the cell to protrude towards the motogenic signal (Small et al., 2002). Stress fibres are long actin filaments linked by

[1]School of Biomedical Sciences, Faculty of Biological Sciences, University of Leeds, Leeds LS2 9JT, UK. [2]Multidisciplinary Cardiovascular Research Centre, University of Leeds, Leeds LS2 9JT, UK.

*Author for correspondence (a.sivaprasadarao@leeds.ac.uk)

A.S., 0000-0002-6755-3502

α-actinin and myosin; contraction of stress fibres enables forwards movement of the cell body (Tojkander et al., 2012). In coordination with the changes in the actin cytoskeleton, focal adhesions undergo cycles of assembly and disassembly to allow adhesion of the front of the cell to the extracellular matrix (ECM) and de-adhesion of the rear of the cell, respectively (Gardel et al., 2010; Turner, 2000). Focal adhesions are physically linked to stress fibres to allow mechanical integration of actin and adhesion dynamics during cell migration (Gardel et al., 2010; Giannone et al., 2007).

A well-documented example of a motogenic signal (chemo-attractant) is H_2O_2 (Hurd et al., 2012; Niethammer et al., 2009; Polytarchou et al., 2005). The mechanism by which H_2O_2 induces cell migration, however, is not fully understood, although H_2O_2 is known to affect a number of signalling pathways associated with cell migration, including Ca^{2+} signalling (Prevarskaya et al., 2011; Tsai et al., 2014; Wei et al., 2012) and Lyn activation (Yoo et al., 2011). Multiple studies have shown that Ca^{2+} plays a key role in the spatial and temporal regulation of the actin cytoskeleton and focal adhesions (Brundage et al., 1991; Gilbert et al., 1994; Prevarskaya et al., 2011; Tsai et al., 2014; Wei et al., 2012).

Here, we asked whether the TRPM2 channel, a member of the transient receptor potential (TRP) family, plays a role in actin and focal adhesion dynamics, and thus in cancer cell migration. The rationale behind this is the fact that TRPM2 channels are strongly activated by H_2O_2 and affect Ca^{2+} signalling (Sumoza-Toledo and Penner, 2011; Takahashi et al., 2011). We examined the role of TRPM2 channels in prostate cancer (PC)-3 and HeLa cell lines. Our results demonstrate that TRPM2 channels indeed mediate the effects of H_2O_2 on cell migration by remodelling the actin cytoskeleton. We found that TRPM2 activation increases the cytosolic levels of not only Ca^{2+}, but also Zn^{2+}, and that Ca^{2+} and Zn^{2+} regulate actin cytoskeleton dynamics, focal adhesion dynamics and cell migration in a reciprocal manner, with Zn^{2+} playing a dominant role.

RESULTS

H_2O_2-induced actin remodelling in cancer cells is dependent on TRPM2 channels

Given that H_2O_2 is cytotoxic and its toxicity can vary depending on the cell type (Manna et al., 2015), we first screened PC-3 and HeLa cells for their sensitivity to H_2O_2 (data not shown) and chose a concentration (<200 μM) that is not cytotoxic under the experimental conditions used. We used Alexa-Fluor-488-conjugated phalloidin, a fluorescent actin stain, to monitor H_2O_2-induced changes in the actin cytoskeleton. The results show that H_2O_2 abolishes stress fibres and generates numerous filopodia in both PC-3 (Fig. 1A) and HeLa (Fig. 1E) cells. In RT-PCR experiments, we demonstrate expression of TRPM2 mRNA in both the cell lines (Fig. S1A). Consistent with the RT-PCR data, an H_2O_2 stimulus caused an increase in cytosolic $[Ca^{2+}]$ that was suppressed by 2-aminoethoxydiphenyl borate (2-APB), an inhibitor of TRPM2 channels (Fig. S1B–E). These data indicate that H_2O_2 causes
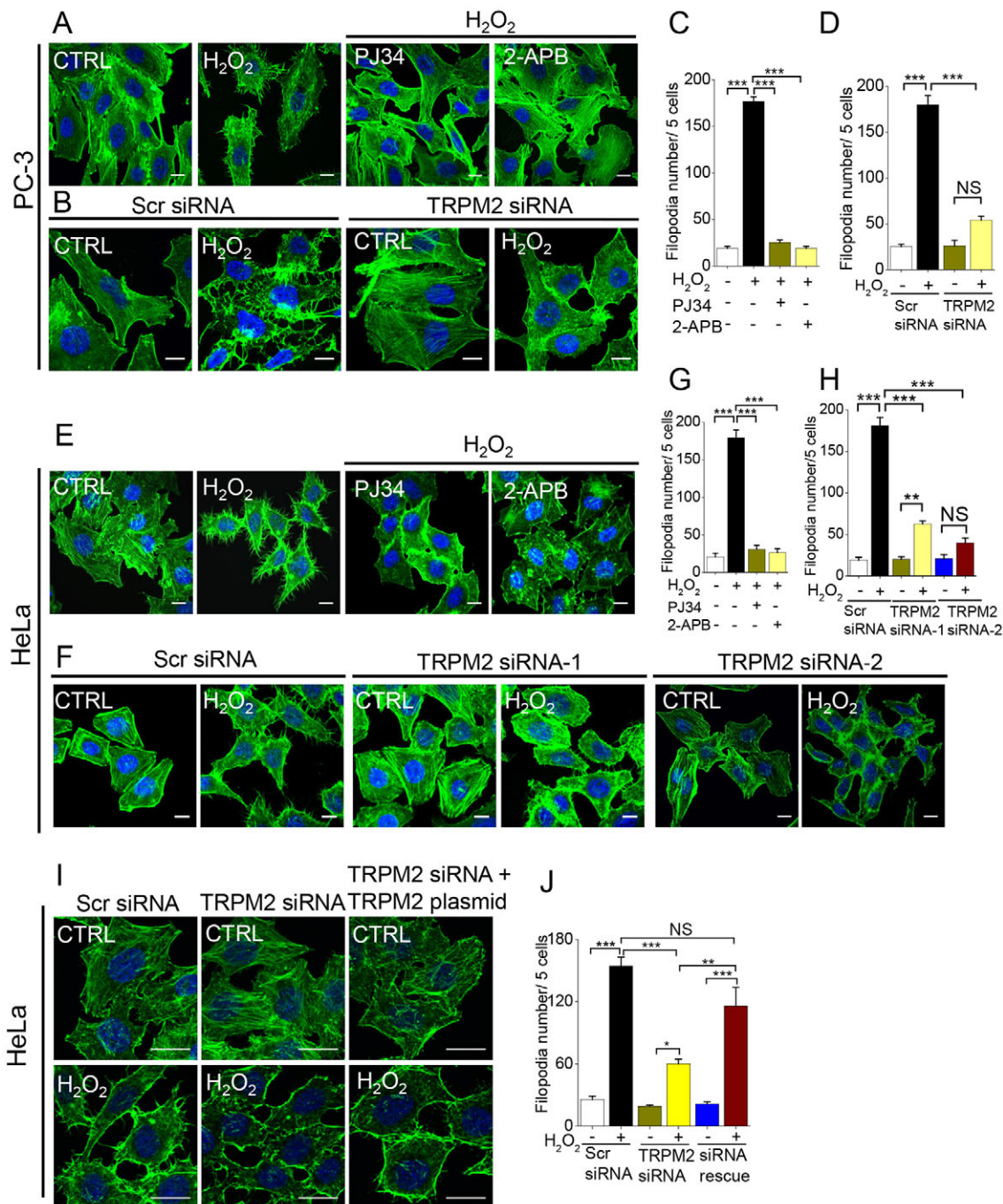
Fig. 1. H₂O₂-induced actin remodelling is dependent on TRPM2 channels. (A) Confocal images of PC-3 cells stained for F-actin following H₂O₂ (100 µM, 2 h at 37°C) treatment in the absence and presence of TRPM2 inhibitors (10 µM PJ34 and 150 µM 2-APB); controls (CTRL) were untreated. (B) Confocal images of untreated (CTRL) and H₂O₂-treated (100 µM, 2 h at 37°C) PC-3 cells stained for actin; cells were transfected with scrambled (Scr) siRNA or TRPM2-targeted siRNA. (C,D) Mean±s.e.m. of filopodia number from experiments performed as in A and B, respectively; *n*=3. (E) Confocal images of HeLa cells subjected to experiments as for A above, except 200 µM H₂O₂ was used. (F) Confocal images of HeLa cells subjected to experiments as for B above, except 200 µM H₂O₂ and a second siRNA (siRNA-2) were used. (G,H) Mean±s.e.m. of filopodia number from experiments performed as in E and F, respectively; *n*=3. (I,J) Rescue of siRNA inhibition of filopodia induction by overexpression of siRNA-resistant TRPM2 plasmid. Images of actin-stained HeLa cells transfected with the indicated siRNA and plasmid constructs exposed to medium alone (CTRL) or medium containing H₂O₂ (I), and the corresponding mean±s.e.m. data (J). Representative images are shown. Scale bars: 10 µm. **P<0.01; ***P<0.001; NS, not significant (one-way ANOVA with Tukey post-hoc test).

extensive remodelling of the actin cytoskeleton in HeLa and PC-3 cells and that both cell lines express H₂O₂-sensitive TRPM2 channels.

Inhibition of TRPM2 channels with PJ34 (another TRPM2 channel inhibitor) and 2-APB abolished the H₂O₂-induced filopodia formation in both PC-3 and HeLa cells (Fig. 1A,C,E,G);

2-APB rescued the H₂O₂-induced loss of stress fibres more effectively than PJ34. Inhibition of TRPM2 channels with N-(p-amylcinnamoyl)anthranilic acid (ACA, 10 µM) produced results similar to those with 2-APB (data not shown). Furthermore, small interfering siRNAs (siRNA-1 and siRNA-2) targeted against TRPM2 channels (Fig. S1F,G), but not the scrambled control

siRNA, suppressed H_2O_2-induced filopodia formation; rescue of stress fibres, however, was partial (Fig. 1B,D,F,H). Ectopic expression of a siRNA-resistant TRPM2 cDNA construct rescued the inhibitory effect of TRPM2 siRNA on filopodia formation (Fig. 1I,J). These data suggest that TRPM2 channels mediate H_2O_2-induced actin cytoskeleton rearrangement. Further experiments into the underlying mechanisms were performed on HeLa cells as these cells showed a better morphology and staining pattern to allow quantifications.

Extracellular Ca²⁺ entry is not essential for actin cytoskeleton remodelling

TRPM2 channels mediate extracellular Ca^{2+} entry (Sumoza-Toledo and Penner, 2011; Takahashi et al., 2011) and, in some cells, lysosomal Ca^{2+} release (Lange et al., 2009). Depletion of extracellular Ca^{2+} failed to prevent H_2O_2-induced filopodia formation (Fig. 2A,B), indicating that extracellular Ca^{2+} entry is not essential for filopodia formation. Interestingly, there was a small, but significant, increase in filopodia in the absence of Ca^{2+} entry; this suggests that maintenance of basal level of cytosolic Ca^{2+} is essential to prevent filopodia formation. Consistent with this interpretation, depletion of intracellular Ca^{2+} with BAPTA-AM induced a significant increase in filopodia formation in the absence of H_2O_2 stimulus (Fig. 2C,D). The effect on stress fibres was less discernible as H_2O_2 treatment in the absence of extracellular Ca^{2+} caused a marked reduction in the projected cell area. We examined the H_2O_2-induced Ca^{2+} changes using Fluo-4. H_2O_2 caused a marked rise in intracellular fluorescence as detected by confocal microscopy (Fig. 2E,F; Fig. S2E) and flow cytometry (Fig. 2G,H). Removal of extracellular Ca^{2+} with EGTA reduced, but failed to abolish the Ca^{2+} signal completely (Fig. 2E,F), indicating that H_2O_2 causes both Ca^{2+} entry and release. The fluorescence signal was abolished by PJ34, 2-APB (Fig. 2E–H) and TRPM2 siRNA (Fig. 2I,J), indicating a role for TRPM2 channels in H_2O_2-induced Ca^{2+} entry and release. Previous studies have reported expression of TRPM2 channels in lysosomes of the INS-1 pancreatic β-cell line and dendritic cells, where they mediated lysosomal Ca^{2+} release (Lange et al., 2009; Sumoza-Toledo et al., 2011). We therefore examined HeLa cells for lysosomal expression of TRPM2 channels. Transiently expressed HA-tagged TRPM2 channels (green) showed colocalisation (yellow in the merged image) with the lysosomal CD63 protein (red) (Fig. 2K). Western blotting of lysosomes isolated from transfected HeLa cells by OptiPrep density gradient centrifugation showed a band corresponding to the estimated size (∼170 kDa) of HA–TRPM2 (Fig. 2L). Taken together, our data suggest that TRPM2 mediates Ca^{2+} entry as well as release, but extracellular Ca^{2+} entry does not contribute to actin remodelling.

H₂O₂ activation of TRPM2 channels induces cytosolic increase of not only Ca²⁺ but also Zn²⁺

It is known that Fluo-4 is not specific for Ca^{2+}; for example, it binds Zn^{2+} ∼100-fold more avidly than Ca^{2+} (Manna et al., 2015; Sensi et al., 2009). We therefore asked whether the Fluo-4 signal seen in Fig. 2E, attributed to Ca^{2+}, could, in part, be due to a rise in Zn^{2+}. Consistent with this hypothesis, we found that the Zn^{2+}-selective chelator TPEN was able to attenuate the Fluo-4 signal, whereas BAPTA-AM, which chelates both Ca^{2+} and Zn^{2+}, abolished the Fluo-4 signal (Fig. S2A,B). Furthermore, using FluoZin-3-AM, a Zn^{2+}-specific fluorophore, we demonstrated an H_2O_2-induced rise in cytosolic $[Zn^{2+}]$ using confocal microscopy (Fig. 3A,B; Fig. S2G) and flow cytometry (Fig. 3C,D). The FluoZin-3–Zn^{2+}

signal was fully prevented by TPEN, but BAPTA-AM failed to quench the signal fully (Fig. S2C,D). Thus, H_2O_2 not only induces a rise in cytosolic $[Ca^{2+}]$ but also in $[Zn^{2+}]$.

Chemical or siRNA-mediated inhibition of TRPM2 channels suppressed the rise in the cytosolic levels of Zn^{2+} (Fig. 3A–F), as well as Ca^{2+} (Fig. 2E–J). Inclusion of EGTA (which can chelate both Ca^{2+} and Zn^{2+}) in the extracellular medium failed to prevent the increase in Zn^{2+} fluorescence indicating Zn^{2+} release from an intracellular source. Co-staining of cells for Zn^{2+} (green) and intracellular organelles (red marker dyes) showed significant colocalisation (yellow in merged images) of Zn^{2+} stain with LysoTracker (Fig. 3G), indicating that the source of the Zn^{2+} is likely lysosomes. Such a conclusion is consistent with the localisation of TRPM2 channels in lysosomes (Fig. 2K,L) and the TRPM2-dependent rise in cytosolic $[Zn^{2+}]$ (Fig. 3). Taken together with the data in Fig. 2, the results show that H_2O_2-mediated activation of TRPM2 channels increases the cytosolic levels of not only Ca^{2+} but also Zn^{2+}.

H₂O₂ induces disassembly of focal adhesions

Studies have shown that loss of stress fibres is accompanied by the simultaneous loss of focal adhesions (Dourdin et al., 2001; Ridley and Hall, 1992; Vicente-Manzanares et al., 2009). We have therefore examined the effect of H_2O_2 on the size and number of focal adhesions by immunostaining for paxillin, an adaptor protein widely used as a focal adhesion marker. Consistent with the expectation, H_2O_2 treatment caused a marked loss of focal adhesions, as well as a decrease in their size (Fig. 4A–C). PJ34 failed to rescue the loss of focal adhesions, but 2-APB was able to prevent H_2O_2-induced loss of focal adhesions (Fig. 4A–C). Knockdown of TRPM2 channels with siRNA significantly rescued focal adhesion density, but not the size of focal adhesions (Fig. 4D–F). These data suggest that TRPM2 channels play a partial role in focal adhesion dynamics and that other mechanisms, including ORAI1–STIM channels (Yang et al., 2009a), contribute to focal adhesion remodelling. Further studies are required to determine the individual contributions of various channels to focal adhesion remodelling.

Ca²⁺ and Zn²⁺ elicit opposite effects on actin remodelling and focal adhesions

To get an insight into the underlying mechanism, we examined the individual roles of Ca^{2+} and Zn^{2+} in actin remodelling and focal adhesions. Chelation of Ca^{2+} with BAPTA-AM had little effect on H_2O_2-induced changes in the actin cytoskeleton (Fig. 5A,B). By contrast, chelation of Zn^{2+} with TPEN completely suppressed the H_2O_2-induced filopodia formation and loss of stress fibres (Fig. 5A,B). Given that H_2O_2 can affect a number of other signalling pathways (Giorgio et al., 2007), which could confound the interpretation of our data, we used Ca^{2+} and Zn^{2+} ionophores, and TPEN, to investigate the individual roles of these two ions in the absence of H_2O_2. Prior to their use, we validated the specificity of the probes (Fig. S3A–D): A23187 caused an increase in cytosolic Ca^{2+}, but not Zn^{2+}; zinc pyrithione (Zn-PTO) caused a rise in cytosolic Zn^{2+}, but not Ca^{2+}; and TPEN, as reported previously (Manna et al., 2015), failed to chelate Ca^{2+}.

Increasing the cytosolic Ca^{2+} levels through treatments with A23187 or thapsigargin (data not shown) had no major effect on actin cytoskeleton, but, interestingly, co-treatment with BAPTA-AM attenuated stress fibres and induced filopodia formation (Fig. 5C,D). Thus, basal levels of Ca^{2+} appear to be essential to maintain stress fibres and to suppress filopodia formation. By
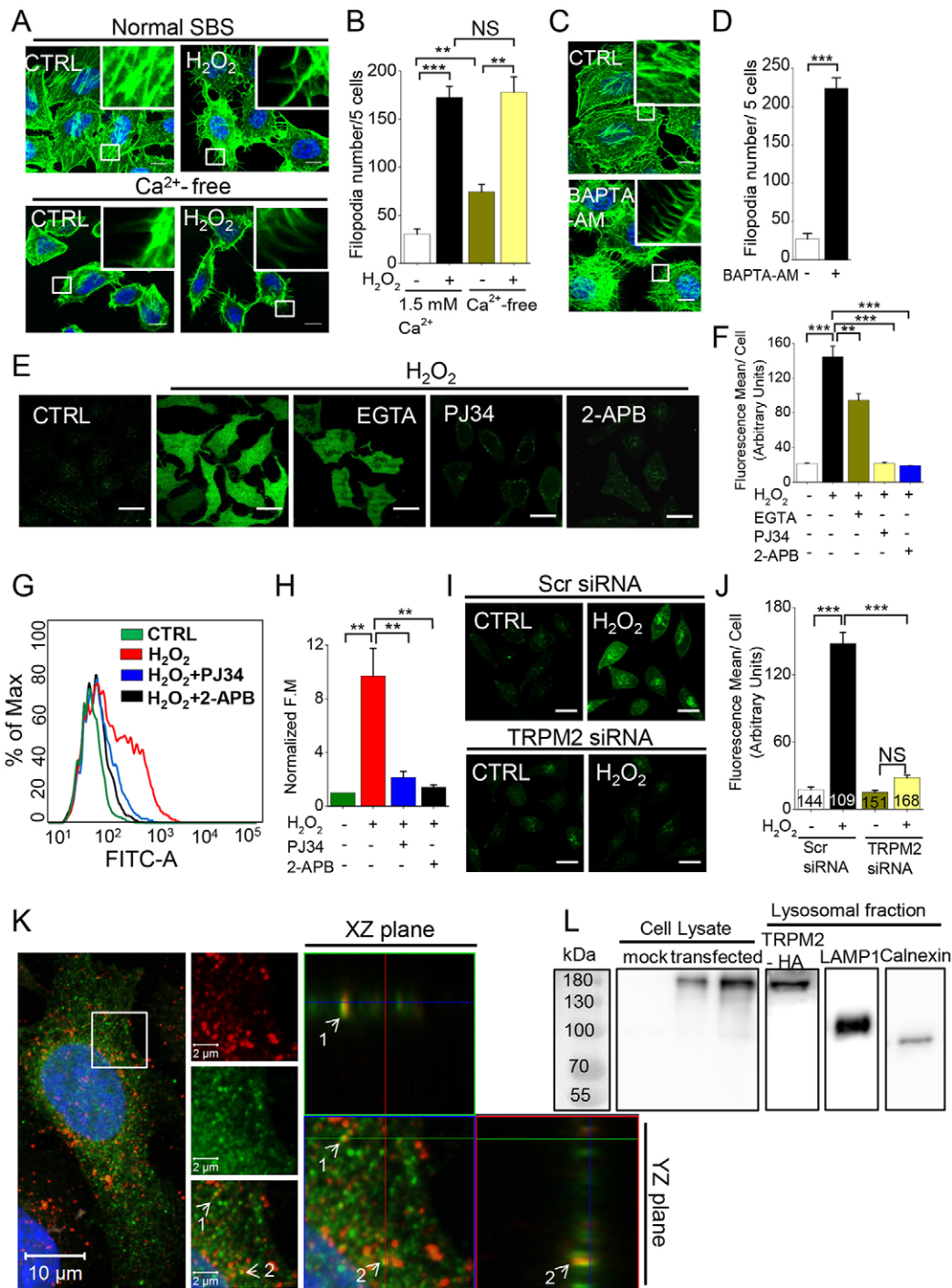
Fig. 2. Depletion of cytosolic Ca²⁺ causes actin remodelling similar to H₂O₂. (A) Confocal images of HeLa cells treated with H₂O₂ (200 µM) in normal SBS (1.5 mM Ca²⁺) or Ca²⁺-free SBS (with 0.4 mM EGTA) for 2 h at 37°C and stained for F-actin; controls were left untreated. (B) Mean±s.e.m. of filopodia number from experiments (n=3) performed as in A. (C) Confocal images of HeLa cells treated with vehicle (CTRL) or BAPTA-AM (10 µM) and stained for F-actin. (D) Mean±s.e.m. of filopodia number from experiments (n=3) performed as in C. (E) Confocal images of HeLa cells either not treated (CTRL) or treated with H₂O₂ (200 µM) with or without EGTA (5 mM), PJ34 (10 µM) and 2-APB (150 µM) and stained with Fluo-4-AM. (F) Mean±s.e.m. of average Ca²⁺ fluorescence per cell from experiments (n=3) performed as in E. (G) HeLa cells were treated as in E, stained with Fluo-4-AM and subjected to FACS (number of cells ≥5000). (H) Mean±s.e.m. data from experiments (n=3) performed as in G confirm a TRPM2-dependent Ca²⁺ rise. (I) H₂O₂-induced Fluo4 signal in HeLa cells is completely suppressed by TRPM2 siRNA. HeLa cells transfected with scrambled siRNA or siRNA against TRPM2 were treated with the medium (CTRL) or medium containing 200 µM H₂O₂ (2 h) before Ca²⁺ imaging; confocal images are shown. (J) Mean±s.e.m. of average fluorescence per cell from three independent experiments (number of cells analysed are shown within each bar) performed as in I. (K) Confocal images of TRPM2–HA-transfected HeLa cells stained for CD63 (red) and the HA tag (green); yellow puncta (shown with arrows) indicate colocalisation of CD63 and the HA tag; orthogonal sections across xz and yz planes are also shown. (L) Detection of TRPM2–HA in the lysosomal fraction of transfected HeLa cells by western blotting. Transfected, but not mock-transfected cells, show a band at ~180 kDa corresponding to TRPM2–HA. Lysosomes isolated by OptiPrep density gradient centrifugation were blotted for TRPM2–HA, LAMP-1 (a lysosomal marker) and calnexin (an ER marker). Insets in A, C and K display enlarged views of boxed regions. Scale bars: 10 µm (A,C); 20 µm (E,I). **P<0.01; ***P<0.001; NS, not significant [one-way ANOVA with Tukey post-hoc test (B,F,H and J) or Student's t-test (D)].
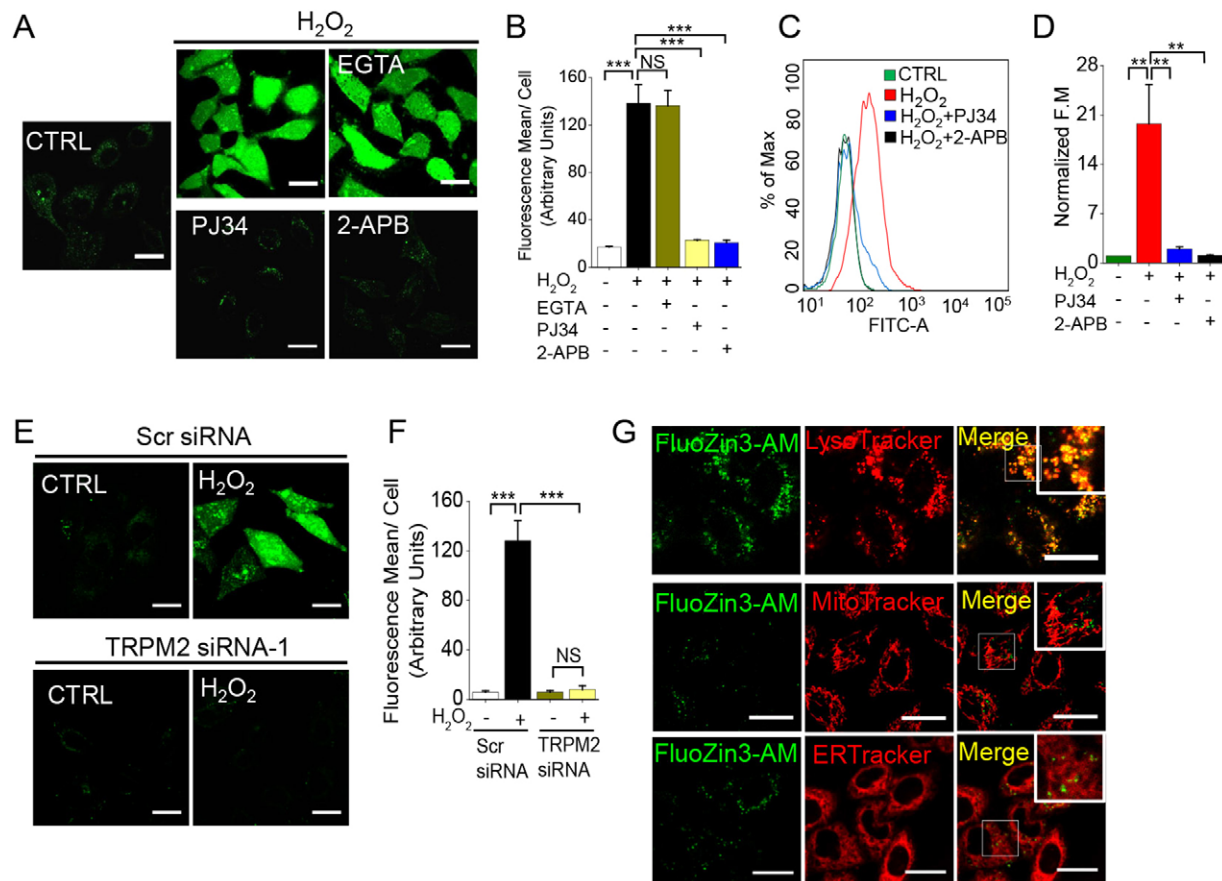
Fig. 3. H$_2$O$_2$ activation of TRPM2 channels causes intracellular Zn^{2+} release with free Zn^{2+} being largely present in lysosomes. (A) Confocal images of HeLa cells treated as in Fig. 2E and stained for Zn^{2+} using FluoZin3-AM. (B) Mean±s.e.m. of average Zn^{2+} fluorescence per cell from experiments (n=3) performed as in A. (C) HeLa cells were treated as in Fig. 2E, stained with FuoZin-3-AM and subjected to FACS (number of cells ≥5000). (D) Mean±s.e.m. data from experiments (n=3) performed as in C. (E) Confocal images of HeLa cells transfected with scrambled (Scr) siRNA or TRPM2 siRNA, and subjected to medium (CTRL) or H$_2$O$_2$ (200 μM) treatment before staining for Zn^{2+}. (F) Mean±s.e.m. data from three experiments (n=3) performed as in E. (G) Confocal images of HeLa cells stained for Zn^{2+} (green) and organelle indicators (red) show the presence of free Zn^{2+} in lysosomes (yellow); boxed regions are enlarged in insets. Scale bars: 20 μm. **P<0.01; ***P<0.001; NS, not significant (one-way ANOVA with Tukey post-hoc test).

contrast, Zn-PTO (2 μM Zn and 6 μM PTO) suppressed stress fibres and increased filopodia formation, whereas co-application of TPEN fully prevented the effects of Zn-PTO (Fig. 5C,D). Control experiments confirmed that PTO (6 μM) and Zn^{2+} (2 μM) had no effect; however, higher concentrations of Zn^{2+} (100 μM), as expected, produced effects similar to Zn-PTO (data not shown). We also used bafilomycin to raise cytosolic Zn^{2+} (Fig. S3F) by inhibiting lysosomal sequestration of the ion (Kukic et al., 2014). Again, this manoeuvre caused loss of stress fibres and appearance of filopodia (Fig. S3E). Taken together, our data demonstrate that Zn^{2+} promotes filopodia formation and disassembly of stress fibres, and that Ca^{2+} and Zn^{2+} have distinct, but opposite, effects on stress fibres and filopodia formation. Interestingly, the effects of Zn-PTO are very similar to those of H$_2$O$_2$, indicating that Zn^{2+}, rather than Ca^{2+}, plays a dominant role in the remodelling of the actin cytoskeleton.

We next examined the individual roles of Ca^{2+} and Zn^{2+} in focal adhesion dynamics. Raising the intracellular [Ca^{2+}] with A23187 had no effect on either the size or the number of focal adhesions (Fig. 5E–G). Chelation of Ca^{2+} with BAPTA-AM significantly reduced the size and number of focal adhesions. By contrast, elevation of cytosolic Zn^{2+} with Zn-PTO led to a significant decrease in the number and size of focal adhesions (Fig. 5E–G). These effects of Zn-PTO were reversed by the co-application of

TPEN. Thus, Ca^{2+} and Zn^{2+} have contrasting effects on the dynamics of focal adhesions: Ca^{2+} supports, whereas Zn^{2+} attenuates, focal adhesion density and size. However, depletion of intracellular Ca^{2+} appears to be more effective in the destabilisation of focal adhesions than the elevation of Zn^{2+}.

Taken together, these data indicate that Ca^{2+} and Zn^{2+} have opposite effects on actin cytoskeleton and focal adhesion dynamics.

H$_2$O$_2$-induced cell migration is TRPM2 dependent

To investigate the relevance of the above findings to cell migration, we used an agarose spot cell migration assay (Fig. 6A) where we included test compounds in the agarose spot and examined the migration of surrounding cells into the spot (Wiggins and Rappoport, 2010). Based on the cellular changes, we predicted that inhibition of TRPM2 channels would eliminate H$_2$O$_2$-induced cell migration, and that Zn^{2+} would promote, but Ca^{2+} would attenuate, cell migration. H$_2$O$_2$ included in the agarose spot would be expected to diffuse into the surrounding medium, enter the cells and induce their migration into the spot. To confirm the H$_2$O$_2$ entry into cells, we stained cells with H2DCF-DA, a reactive oxygen species (ROS) detection reagent. Consistent with the expectation, cells near the boundary of an agarose spot containing H$_2$O$_2$, but not one containing PBS, displayed significantly greater levels of staining compared to cells away from the spot (Fig. 6B,C). The
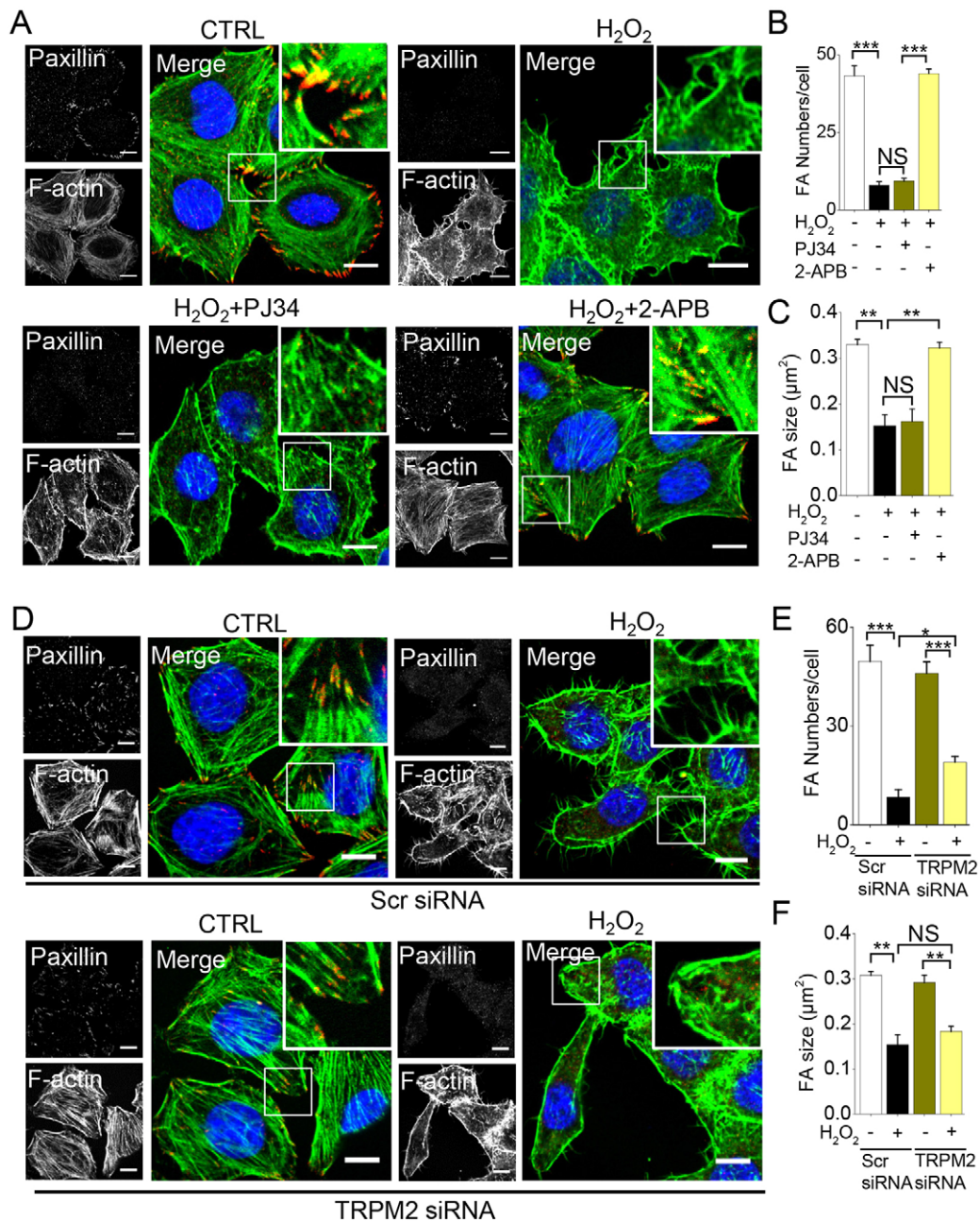
Fig. 4. Focal adhesion disassembly is mediated by TRPM2 channels. (A) Confocal images of HeLa cells stained for F-actin (green) and paxillin (red) following vehicle (CTRL) or H_2O_2 (200 µM) treatment in the absence and presence of PJ34 (10 µM) or 2-APB (150 µM). (B,C) Mean±s.e.m. of average focal adhesion (FA) number (B) and size (C) per cell from experiments (n=3) performed as in A. (D) Confocal images of HeLa cells transfected with scrambled (Scr) siRNA or TRPM2 siRNA; cells were treated with vehicle (CTRL) or H_2O_2 (200 µM) and stained for F-actin and paxillin. (E,F) Mean±s.e.m. of average focal adhesion number (E) and size (F) from experiments (n=3) performed as in D. Insets in A and D display enlarged views of boxed regions. Scale bars: 10 µm. *P<0.05; **P<0.01; ***P<0.001; NS, not significant (one-way ANOVA with Tukey post-hoc test).

results show that inclusion of H_2O_2 in the agarose spot promoted migration of cells into the spot; there was little migration in the PBS controls (Fig. 6D; Fig. S4A). 2-APB prevented H_2O_2-stimulated cell migration (Fig. 6D,E; Fig. S4A,B). siRNA targeted against TRPM2 channels, but not scrambled siRNA, as predicted, prevented H_2O_2-induced cell migration (Fig. 6F–I; Fig. S4C,D). These results demonstrate that TRPM2 channels mediate H_2O_2-induced directional migration of HeLa and PC-3 cells. The lack of effect of PJ34 proved to be anomalous, because PJ34 stimulated cell migration even in the absence of H_2O_2 (Fig. S4E–H). This can be attributed to TRPM2-independent effects of PJ34, as reported

previously (Mathews and Berk, 2008). This finding might be of clinical relevance because poly(ADP-ribose) polymerase (PARP) inhibitors are currently being evaluated for cancer therapy (Michels et al., 2014). To further confirm the role of TRPM2 channels in cell migration, we used a recombinant approach. Our results show that overexpression of TRPM2 channels led to a significant increase in H_2O_2-induced migration of HEK-MSR cells (Fig. S4I,J). Collectively, our data demonstrate that TRPM2 channels mediate H_2O_2-induced directional cell migration.

Given that TRPM2 channels mediate their effects through Ca^{2+} and Zn^{2+}, we tested the individual roles of these ions using
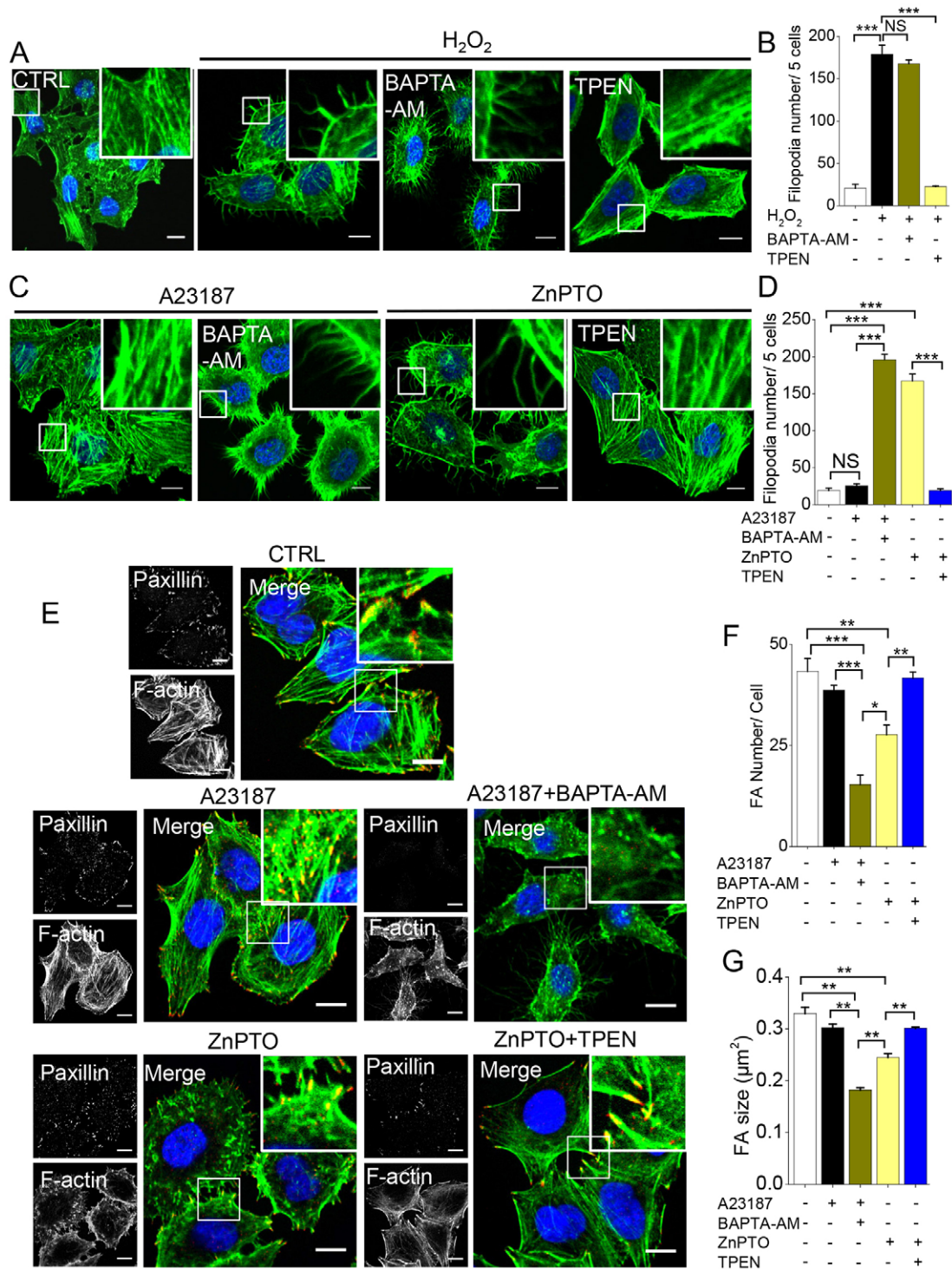
Fig. 5. Opposite effects of Ca^{2+} and Zn^{2+} on H_2O_2-induced actin remodelling and focal adhesions. (A,D) Effects of Ca^{2+} and Zn^{2+} on actin remodelling. (A) Confocal images of HeLa cells either not treated (CTRL) or treated with H_2O_2 (200 μM) with or without BAPTA-AM (10 μM) and TPEN (10 μM) and stained for actin. (B) Mean±s.e.m. data from experiments (n=3) performed as in A. (C) Confocal images of HeLa cells treated A23187 (3 μM) with or without BAPTA-AM (10 μM), or Zn-PTO (3 μM) with or without TPEN (10 μM). (D) Mean±s.e.m. data from experiments (n=3) performed as in C. Insets in A and C display enlarged views of boxed regions. (E,G) Effects of Ca^{2+} and Zn^{2+} on focal adhesion remodelling. (E) Confocal images of HeLa cells stained for F-actin and paxillin following vehicle (CTRL), A23187 (3 μM) minus or plus BAPTA-AM (10 μM); or Zn-PTO (3 μM) minus or plus TPEN (10 μM) treatments. (F,G) Mean±s.e.m. of average focal adhesion (FA) number (F) and size (G) per cell from experiments (n=3) performed as in E. Insets display enlarged views of boxed regions. Scale bars: 10 μm. *P<0.05; **P<0.01; ***P<0.001; NS, not significant (one-way ANOVA with Tukey post-hoc test).

ionophores and metal chelators in the absence of H_2O_2. A23187 showed no effect, whereas inclusion of BAPTA-AM caused a modest, but significant, increase in HeLa cell migration (Fig. 6J,K).

Zn-PTO, by contrast, strongly promoted cell migration that was suppressed by TPEN (Fig. 6J,K). These data suggest that Ca^{2+} and Zn^{2+} play distinct, but contrasting, roles in cell migration.
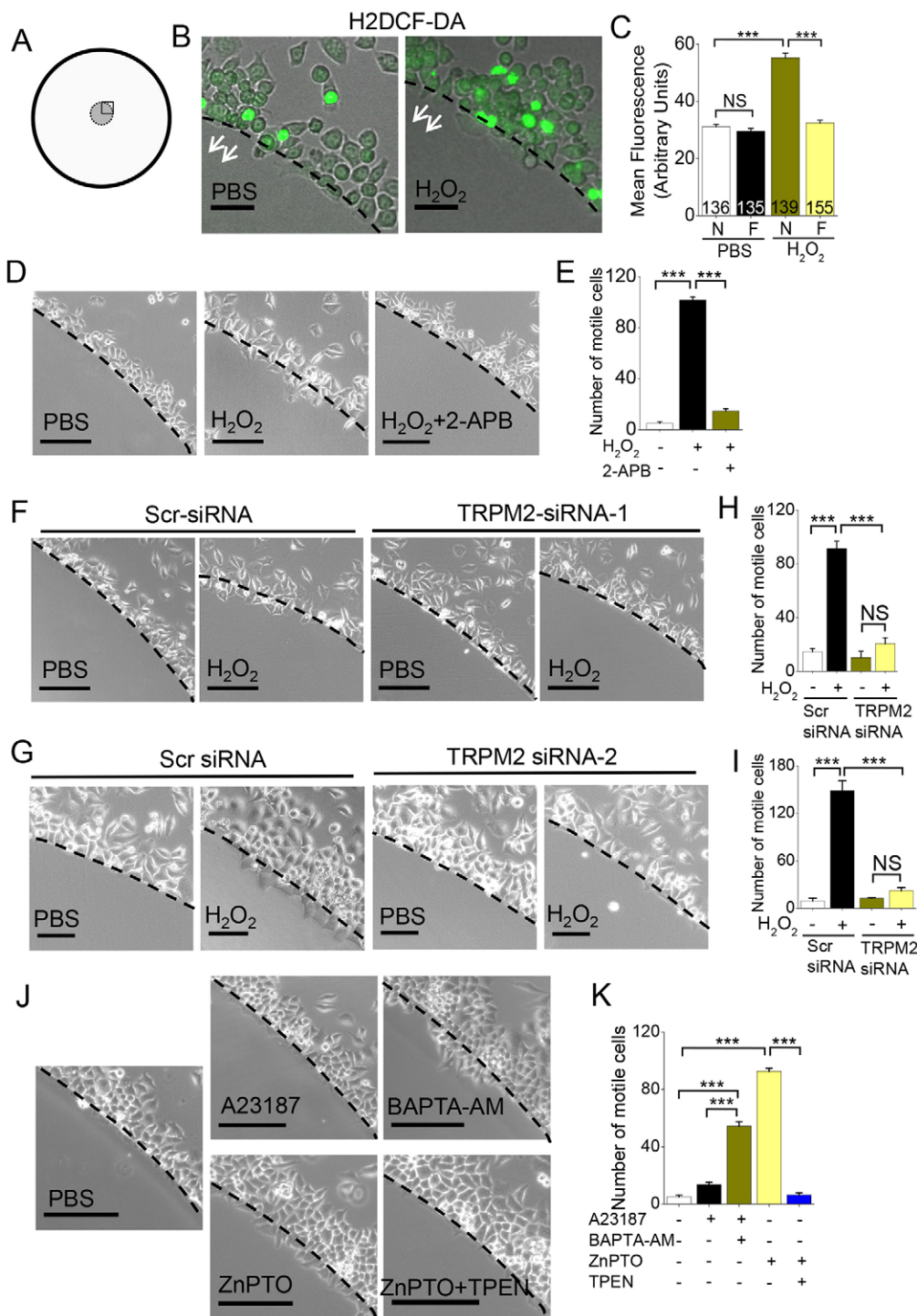
Fig. 6. H2O2-induced directional migration is TRPM2 and Zn2+ dependent. (A) Schematic illustrating an agarose bead (broken circle) in the centre of a Petri dish around which cells are plated; the square box represents the section imaged. (B) Representative images of HeLa cells migrating (6 h) towards agarose spots containing PBS or H_2O_2 (1 mM) stained with H2DCF-DA. The white arrows indicate the direction of migration across the boundary of the agarose spot shown as a dashed curve. Scale bars: 20 μm. (C) Mean± s.e.m. of fluorescence of cells on, or touching, the boundary (N) or away (F) from the boundary (between 30 and 100 μm). Bright green cells (presumed dead) were excluded from the quantification. The number of cells analysed from three independent experiments are shown within the bar. (D) Images of HeLa cells migrating (after 16 h) towards agarose spots containing PBS, H_2O_2 (1 mM), or H_2O_2 (1 mM) plus 2-APB (150 μM). (E) Mean ±s.e.m. of number of cells that crossed the agarose boundary from experiments (n=3) performed as in D. (F,G) Images of migrating HeLa cells transfected with scrambled siRNA (Scr), or siRNA-1 (F) or siRNA-2 (G), against TRPM2. (H,I) Mean±s.e.m. of number of cells that crossed the agarose boundary from experiments (n=3) performed as in F and G, respectively. (J) Images of HeLa cells migrating towards agarose spots containing PBS, A23187 (5 μM), BAPTA-AM (15 μM), or Zn-PTO (5 μM) with and without TPEN (10 μM). (K) Mean±s.e.m. of number of cells that crossed the agarose boundary from experiments (n=3) performed as in J. In all cases, the dashed line indicates the agarose boundary. Scale bars: 200 μm (D,F,G,J). ***P<0.001; NS, not significant (one-way ANOVA with post-hoc Tukey test).

H2O2 induces migration of lysosomes to the leading edge of the cell

Given that filopodia are formed at the leading edge of migrating cells, and a rise in Zn^{2+} triggers filopodia formation, we would expect preferential Zn^{2+} release to occur at the leading edge of the cell. Given the evidence that lysosomes are the major source of intracellular free Zn^{2+} (Fig. 3G), we predicted that lysosomes move towards the leading edge of the cell. To test this idea, we transfected HeLa cells with tdTomato–F-actin-P (ITPKA-9-52) (Johnson and Schell, 2009) and LAMP1–GFP (to label lysosomes) and imaged migrating cells at the boundary of the agarose spot. The results (Fig. 7A–C) showed that there was a marked accumulation of lysosomes at the leading edge of cells migrating into the H_2O_2-containing agarose spot. Furthermore, these cells showed numerous actin-stained filopodia at the leading edge. By contrast, in control experiments, neither lysosomal trafficking nor filopodia formation was observed. These data indicate that lysosomes migrate towards the leading edge of cells in response to the H_2O_2 stimulus, presumably to increase the local concentration of Zn^{2+}. Interestingly, H_2O_2-induced polarisation of lysosomes was inhibited by TRPM2 siRNA, but not scrambled siRNA (Fig. 7D,E). How TRPM2 channels regulate lysosome migration remains to be investigated.
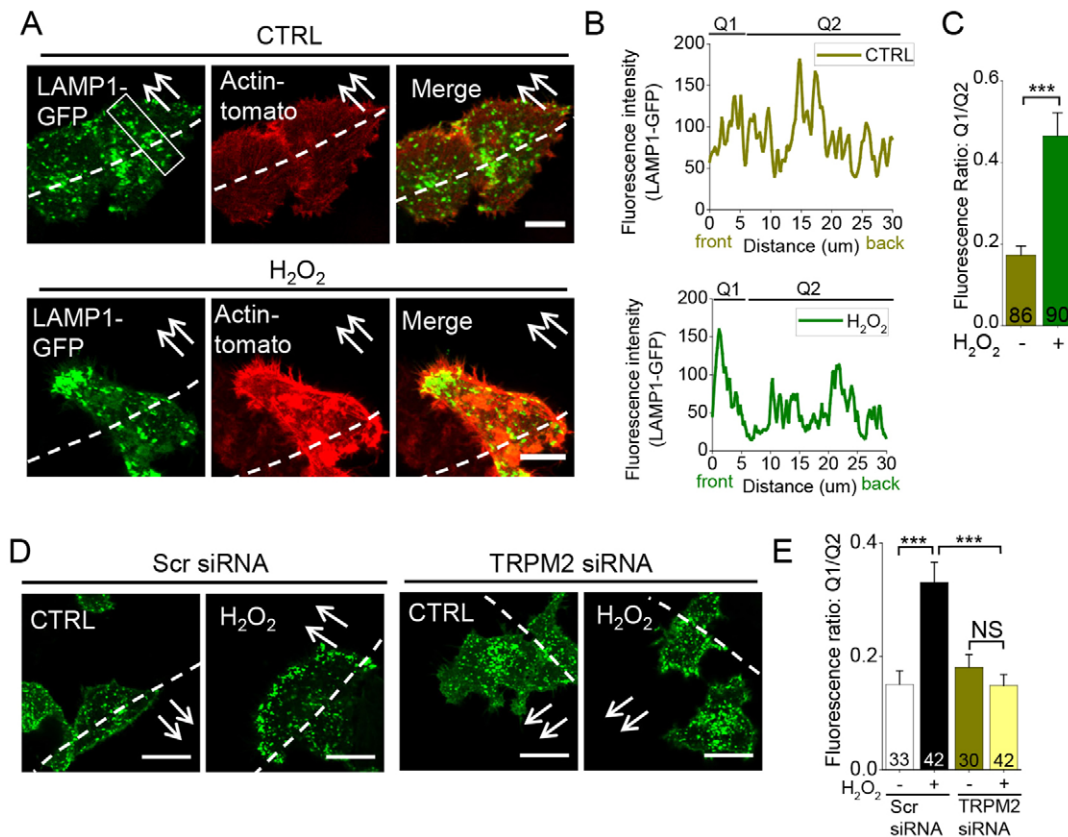
Fig. 7. H$_2$O$_2$ causes polarisation of lysosomes to the leading edge of migrating cells. (A) Confocal images of HeLa cells co-transfected with LAMP1–GFP and actin–td-tomato migrating towards agarose spots containing PBS (CTRL) or H$_2$O$_2$ (1 mM). The white arrows indicate direction of migration across the boundary of the agarose spot shown as a dashed curve. (B) Plot of fluorescence intensity of LAMP1–GFP-positive puncta along the migrational axis of a single cell (indicated as a rectangle in A). (C) Ratio of LAMP1–GFP fluorescence at the leading edge (Q1) relative to the rest of the cell (Q2), where Q1 is fluorescence intensity at the leading edge (0–5 µm, arbitrary) of the cell and Q2, fluorescence intensity behind the leading edge (5–30 µm). (D) Confocal images of HeLa cells co-transfected with LAMP1–GFP and scrambled (Scr) siRNA or TRPM2 siRNA migrating towards agarose spots containing PBS (CTRL) or H$_2$O$_2$ (1 mM); for details see A. (E) Quantification of the ratio of Q1 to Q2 analysed as for C. Data in C and E are mean±s.e.m.; number of cells analysed from three independent experiments are shown within the bars. Scale bars: 20 µm. ***$P<0.001$; NS, not significant [Student's t-test (C) or one-way ANOVA with post-hoc Tukey test (E)].

Role of Rho family GTPases in H$_2$O$_2$-dependent changes in cellular phenotype

Rho family GTPases play crucial roles in cell migration. Rho GTPases regulate stress fibres, whereas Rac and Cdc42 GTPases regulate lamellipodia and filopodia formation, respectively. The action of Rho GTPases is mainly mediated by the Rho-associated coiled-coil-forming protein serine/threonine kinase (ROCK) proteins (Ridley, 2001). We used the ROCK inhibitor Y27632 (Somlyo et al., 2000) to investigate the role of Rho GTPase in cell migration. The results (Fig. 8A,B) show that Y27632 completely inhibited H$_2$O$_2$-induced HeLa cell migration. Furthermore, H$_2$O$_2$-induced movement of lysosomes to the leading edge of migrating cells was also significantly attenuated by Y27632 (Fig. 8C,D). These data indicate that the H$_2$O$_2$-induced cellular changes and cell migration are mediated by the activation of classical Rho-GTPase-dependent pathway.

To examine the role of Cdc42, we tested the ability of a dominant-negative (T17N) form of the eGFP–Cdc42 construct to inhibit H$_2$O$_2$-induced filopodia formation. The results show that expression of this dominant-negative construct failed to prevent H$_2$O$_2$-induced filopodia formation (Fig. 8E). The constitutively active (Q42L) eGFP–Cdc42 construct was able to induce short filopodia in the absence of H$_2$O$_2$ (Fig. 8E). Mellor and colleagues have reported a role for Rif GTPase in filopodia formation in HeLa cells (Ellis and

Mellor, 2000). However, expression of dominant-negative (T17N) Rif GTPase also failed to prevent H$_2$O$_2$-induced filopodia formation (Fig. 8F). The constitutively (Q61L) active Rif GTPase was able to reinforce stress fibres and induce filopodia in non-treated control cells (Fig. 8F), as reported previously (Ellis and Mellor, 2000; Fan et al., 2010). These results suggest that neither the classical Cdc42 nor Rif GTPase is involved in H$_2$O$_2$-induced filopodia formation.

DISCUSSION

Directional cell migration involves repeated cycles of protrusion at the front and retraction at the back of the cell (Gardel et al., 2010; Lamalice et al., 2007; Ridley et al., 2003). These cycles are driven by spatio-temporal remodelling of the actin cytoskeleton and focal adhesions (Gardel et al., 2010; Lamalice et al., 2007; Mattila and Lappalainen, 2008; Ridley et al., 2003; Small et al., 2002; Tojkander et al., 2012). Ca^{2+} is widely regarded as an important coordinator of these events (Prevarskaya et al., 2011; Tsai et al., 2014; Wei et al., 2009, 2012). Accordingly, multiple Ca^{2+} channels and pumps have been implicated in the cell migration (Prevarskaya et al., 2011). They contribute to a rear-to-front global Ca^{2+} gradient (opposite to the direction of cell migration) and generate spatio-temporal Ca^{2+} flickers at the front of the cell, which, in turn, enable remodelling of the molecular machinery responsible for directional cell migration (Wei et al., 2012). However, as will be discussed
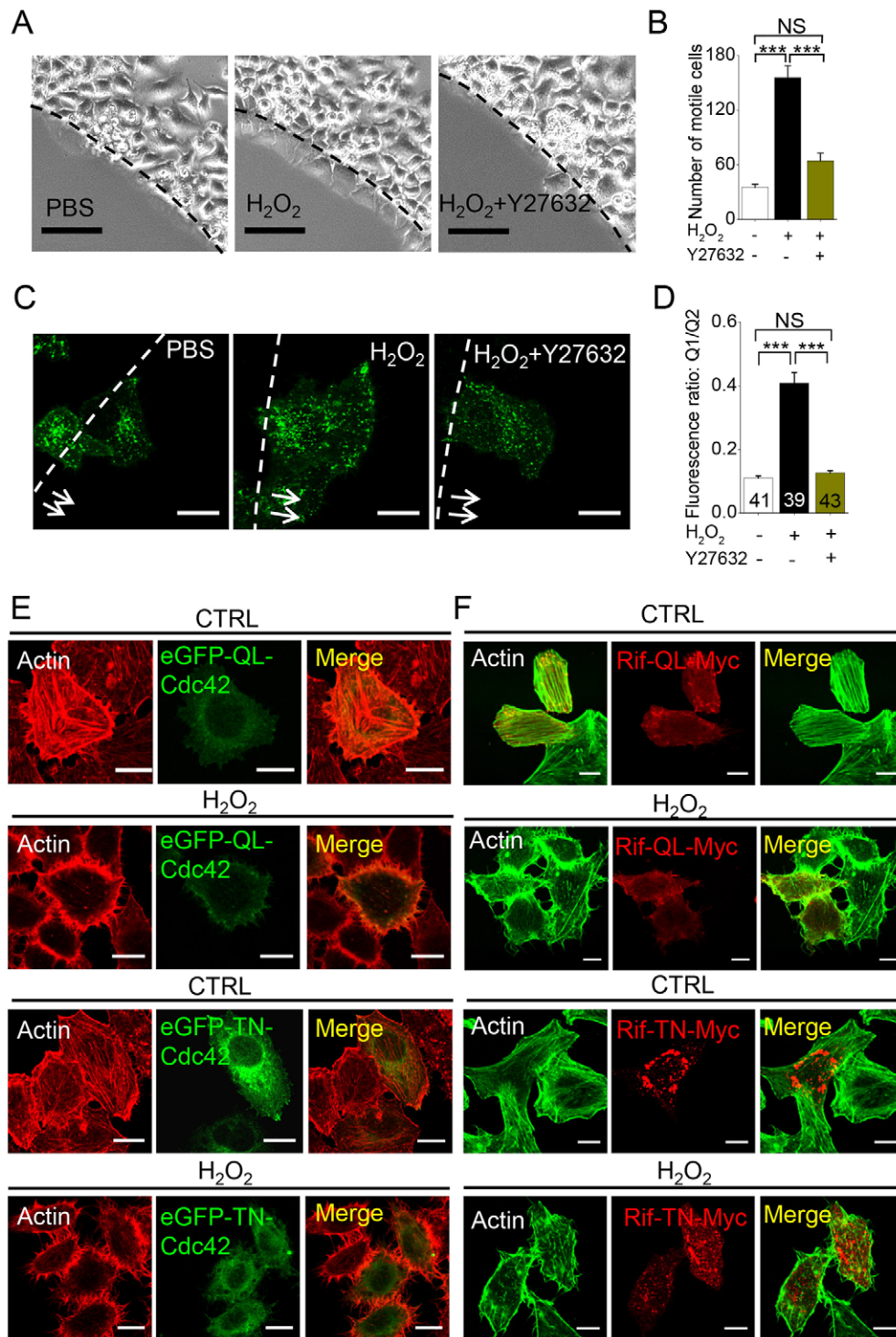
Fig. 8. Role of Rho family GTPases in H_2O_2 induced effects. (A,B) Representative images of HeLa cells migrating in response to H_2O_2 and H_2O_2 plus the Rho kinase inhibitor Y27632 (A) and the corresponding mean ±s.e.m. data (B); n=3; ***P<0.001. (C,D) Effect of Y27632 on lysosomal migration determined as described in Fig. 7; representative images (C) and the corresponding mean±s.e.m. data (D) are shown; Q1/Q2 represents the density of lysosomes at the leading edge of migrating cells relative to the rest of the cells as explained in the legend to Fig. 7; n=3. (E) HeLa cells transfected with eGFP-tagged QL-Cdc42 or TN-Cdc42 plasmids were exposed to medium alone (CTRL) or medium containing H_2O_2 (200 µM, 2 h at 37°C), following which cells were stained for F-actin. (F) HeLa cells transfected with Myc-tagged Rif-QL or Rif-TN were either not treated (CTRL) or treated with medium containing H_2O_2 (200 µM) for 2 h at 37°C. Following this, cells were stained for Myc tag (Rif) and F-actin. Representative confocal images (from three independent experiments) are shown. Scale bars: 20 µm. ***P<0.001; NS, not significant (one-way ANOVA with post-hoc Tukey test).

below, not all findings can be explained in terms of a single model as different cell types employ different mechanisms to regulate migration.

Here, we set out to examine the role of Ca^{2+} in the migration of PC-3 and HeLa cells in response to a H_2O_2 stimulus. H_2O_2 treatment caused a marked loss of stress fibres (Fig. 1A,C,E,G) and focal adhesions (Fig. 4A–C), and induced numerous filopodia (Fig. 1A,C,E,G). Consistent with these changes, there was increased cell migration (Fig. 6D,E; Fig. S4A,B). However, in addition to the suspected increase in cytosolic $[Ca^{2+}]$ (Fig. 2E– H), H_2O_2 caused a marked rise in cytosolic $[Zn^{2+}]$ (Fig. 3A–D). Most unexpectedly, depletion of Zn^{2+} alone was found to be sufficient to prevent all of the H_2O_2-induced changes (Fig. 5A,B). This is an important finding because, up until now, all reports have implicated Ca^{2+} as the primary regulator of cell migration (Prevarskaya et al., 2011; Wei et al., 2012).

Inspired by the unexpected findings, we examined the individual roles of Ca^{2+} and Zn^{2+}. Elevation of global cytosolic $[Ca^{2+}]$ with A23187 had little effect on the actin cytoskeleton (Fig. 5C,D) and focal adhesions (Fig. 5E–G). By contrast, reducing the basal $[Ca^{2+}]$

with BAPTA-AM caused marked loss of stress fibres (Fig. 5C,D) and focal adhesions (Fig. 5E–G), but induced filopodia (Fig. 5C,D) – effects that are similar to those caused by H_2O_2 (Fig. 1). Consistent with these changes, BAPTA-AM increased the rate of cell migration, but A23187 had little effect (Fig. 6J,K). Elevation of cytosolic $[Zn^{2+}]$ with Zn-PTO produced effects that were almost identical to those caused by Ca^{2+} depletion (Figs 5C,D, 6J,K) and H_2O_2 (Figs 1A,C,E,G, 6D,E). Collectively, these findings argue that Zn^{2+}, and not Ca^{2+}, plays the primary role in cell migration in this system. More importantly, a rise in cytosolic $[Zn^{2+}]$ produced an effect equivalent to the decrease in basal $[Ca^{2+}]$. This has led us to the fundamentally important conclusion that Zn^{2+} can antagonise the effects of Ca^{2+} on cellular events regulating cell migration and that it is the ratio of Ca^{2+} to Zn^{2+} in the cell that regulates cell migration, rather than either ion on their own.

The antagonistic role of Zn^{2+} is physiologically relevant because the H_2O_2-induced Zn^{2+} rise (Fig. 3A–D), like the Ca^{2+} rise (Fig. 2E–H), is dependent on the activation of TRPM2 channels. siRNA-mediated silencing or chemical inhibition of TRPM2 channels prevented the H_2O_2-induced rise in Ca^{2+} (Fig. 2E–J) and Zn^{2+} (Fig. 3A–F), remodelling of the actin cytoskeleton (Fig. 1) and cell migration (Fig. 6D–I). Importantly, the effects of TRPM2 inhibition were similar to those of Zn^{2+} depletion (Figs 1, 5 and 6). These results confirm the primary role of Zn^{2+} in H_2O_2-induced cell migration and its physiological relevance. Whether Zn^{2+} plays a similar role in cell migration induced by other migration-promoting signals, and in the migration of other cell types, remains to be investigated. Furthermore, although a role for the TRPM2 channel, and for Zn^{2+}, are clear, and H_2O_2-induced elevation of cytoplasmic Zn^{2+} could be demonstrated using fluorescent probes, it has proved difficult to demonstrate permeability of the channel to Zn^{2+} by electrophysiology (Manna et al., 2015; Yang et al., 2011). Thus, mechanisms other than direct Zn^{2+} permeation by the channel cannot be excluded.

It is important to recognise the fact that the majority of previous studies have used chemical probes to infer a role for Ca^{2+} in cell migration. One of the drawbacks of these probes is that they have a significantly greater affinity (up to 100-fold) for Zn^{2+} than for Ca^{2+} (Manna et al., 2015; Sensi et al., 2009). As such, use of these probes could potentially mask the effects of Zn^{2+}. In this study, we have demonstrated a role for Zn^{2+} in cell migration using Zn^{2+}-specific probes. Furthermore, the role of Zn^{2+} was tested in the absence of H_2O_2 to exclude any confounding effects from the oxidant. The profound effect that Zn^{2+} has on the actin and focal adhesion dynamics is expected to have implications for migration of other cell types where motogenic signals could affect channels and transporters capable of affecting Zn^{2+} homeostasis.

Cytoplasmic levels of Zn^{2+} are tightly regulated by transporters that include members of ZIP (ZRT IRT-like protein) and ZnT (zinc transporter) families that facilitate Zn^{2+} influx and efflux, respectively (Eide, 2006). In addition, there are a number of nonselective cation channels capable of permeating Zn^{2+} ions (Nilius and Szallasi, 2014). Unfortunately, little is known about the role of these Zn^{2+}-handling proteins in cell migration. One recent study has demonstrated that MCF-7 breast cancer cell migration induced by a high glucose concentration is mediated by the ZIP6- and ZIP10-dependent increase in cytosolic Zn^{2+} (Takatani-Nakase et al., 2014). By contrast, there are numerous studies on the role of Ca^{2+} channels in cell migration. However, the effects they have on cell migration are highly variable. For example, activation of TRPC1 (Fabian et al., 2008), TRPC5 (Tian et al., 2010), TRPV1 (Waning et al., 2007) and TRPV2 (Monet et al., 2010) channels

promotes cell migration, whereas activation of TRPC6 (Tian et al., 2010) and TRPM1 (Duncan et al., 1998) reduces cell migration. Even more intriguingly, the same channel can elicit different effects in different cell types. Thus TRPM8 activation stimulates migration of DBTRG glioblastoma cells (Wondergem et al., 2008), but suppresses migration of transfected PC-3 cells (Yang et al., 2009b). TRPM7 activation increases migration of cancer cells (Wei et al., 2009), but inhibits endothelial cell migration (Zeng et al., 2015). Ca^{2+} influx through ORAI1–STIM1 channels promotes migration of cancer cells (Chen et al., 2011; Yang et al., 2009a) and smooth muscle cells (Potier et al., 2009), but inhibits endothelial cell migration (Tsai et al., 2014). How the same Ca^{2+} signal could generate such diverse, even opposite, effects is not known, but it might be possible to reconcile some of these differences if the ability of some of these channels and cell types to also regulate Zn^{2+} dynamics is re-examined. Consistent with this idea is the fact that many of the channels associated with cell migration are not selective for Ca^{2+}; for example, TRPM7 and TRPC6, and some voltage-gated Ca^{2+} channels, can also conduct Zn^{2+} (Nilius and Szallasi, 2014).

We consider the potential implications of our findings to the current model (Tsai et al., 2014; Wei et al., 2012; Yang et al., 2009a) of how Ca^{2+} regulates migration. The model implies generation of Ca^{2+} flickers at the leading edge of the cell against a background of a Ca^{2+} gradient. Precisely how the Ca^{2+} gradient and flickers regulate the molecular processes differently at the front and back of the cell is not clearly understood. The prevailing notion is that high levels of Ca^{2+} at the rear of the cell support myosin-mediated contraction of actin stress fibres and calpain-mediated disassembly of focal adhesions required for rear retraction (Prevarskaya et al., 2011; Tsai et al., 2014; Wei et al., 2012). At the leading edge, where Ca^{2+} levels are low, spatio-temporally generated Ca^{2+} flickers enable a local increase in Ca^{2+} (Ca^{2+} microdomains) to promote actomyosin contraction and focal adhesion disassembly required for protrusion (Prevarskaya et al., 2011; Tsai et al., 2014; Wei et al., 2012). A key requirement of the model is the need to reduce Ca^{2+} levels to below the basal levels in order to induce cytoskeletal and focal adhesion changes. In endothelial cells, plasma membrane Ca^{2+} ATPase (PMCA, also known as ATP2B) has been shown to reduce the Ca^{2+} levels at the front of the cells (Tsai et al., 2014). Whether PMCA contributes to the Ca^{2+} gradient in other cell types is not known, but our discovery that Zn^{2+} can antagonise the effects of Ca^{2+} could offer a solution to the problem.

Thus, it is possible to conceive that a front-to-rear Zn^{2+} gradient could produce the same effect as the rear-to-front Ca^{2+} gradient in a migrating cell. Although we have no direct data to support such Zn^{2+} polarisation, we were able to demonstrate remarkable mobilisation of Zn^{2+}-enriched lysosomes to the leading edge of a migrating cell (Fig. 7). These lysosomes could potentially release Zn^{2+} to raise local (Zn^{2+} microdomains) or global $[Zn^{2+}]$ at the front of the cell to influence events required for cell protrusion. Consistent with this possibility, we found high levels of Zn^{2+}-inducible filopodia at the leading edge of the cell, but these were absent at the rear (Fig. 7). A rise in Zn^{2+} could also provide a counter-regulatory mechanism by which Ca^{2+} signals could be readily terminated. A reduced number of lysosomes at the rear of the cell would ensure low $[Zn^{2+}]$ to sustain Ca^{2+}-dependent stress fibres and adhesions that are essential during the early stages of cell migration. A potential advantage of our Zn^{2+} gradient model is the fact that it allows high $[Ca^{2+}]$ to be maintained to support important Ca^{2+}-dependent events such as myosin-mediated force generation. The molecular basis for how the balance between Ca^{2+}

and Zn^{2+} signalling regulates actin cytoskeleton and focal adhesion dynamics in a spatio-temporal manner, however, remains to be investigated. Likewise, there is a need to demonstrate putative Zn^{2+} gradients in migrating cells.

Cell migration is regulated by the Rho family GTPases, including Rho, Rac and Cdc42. Rho regulates stress fibres, whereas Rac regulates lamellipodia and Cdc42 controls filopodia formation (Ridley, 2001; Ridley et al., 2003). Studies by Mellor and colleagues have reported that Rif GTPases represent an alternative signalling route for filopodia formation (Ellis and Mellor, 2000). A role for Rho signalling in H_2O_2-induced cell migration as well as polarisation of lysosomes was confirmed using the ROCK inhibitor Y27632 (Fig. 8A–D). However, we were unable to demonstrate a role for either Cdc42 or Rif GTPase in H_2O_2-induced cell migration (Fig. 8E,F). Although this was unexpected, Morris and colleagues have reported a Cdc42- and Rif-independent mechanism, involving a lipid-phosphatase-related protein in filopodia formation (Sigal et al., 2007). Further investigations into such Cdc42- and Rif-independent mechanisms are required to appreciate how H_2O_2 induces filopodia formation in these cells.

In conclusion, our study revealed a heretofore unrecognised role for Zn^{2+} in H_2O_2-induced cell migration and a role for TRPM2 channels. The relevance of TRPM2 channels to cancer is underpinned by the fact that TRPM2 expression is upregulated in both prostate and cervical cancer (http://www.proteinatlas.org/ENSG00000142185-TRPM2/cancer). We showed that Zn^{2+} is capable of antagonising the effects of Ca^{2+} on actin cytoskeleton and focal adhesion dynamics, and on cell migration. We also demonstrated that Zn^{2+}-enriched lysosomes migrate towards the chemoattractant H_2O_2, presumably to increase Zn^{2+} levels at the leading edge of the cell and influence the events there. Further studies, including the identification of molecular targets of Zn^{2+}, are required for a meaningful appreciation of the interplay between Ca^{2+} and Zn^{2+} signalling in cancer cell migration. Whether a similar interplay regulates migration of neuronal growth cones and macrophages also remains to be investigated. Finally, from a translational perspective, our study revealed two potential therapeutic opportunities for prevention of metastatic progression of cancer: TRPM2 inhibitors, and chelators capable of removing the free (toxic) form of Zn^{2+}, while sparing the protein-bound essential Zn^{2+}.

MATERIALS AND METHODS
Molecular probes and reagents
LysoTracker Red, MitoTracker Red and ER-tracker Red, Alexa-Fluor-488-conjugated phalloidin, Alexa-Fluor-633-conjugated phalloidin, Pluronic F127, Fura-2AM, Fluo-4-AM, FluoZin-3-AM, SuperScript ii reverse transcriptase, Lipofectamine 2000 and tissue culture media were purchased from Life Technologies. All other chemicals and reagents were from Sigma-Aldrich or Calbiochem. siRNA-1 (ON-TARGETplus Human TRPM2, 7226) was from Thermo Scientific. siRNA-2 (5′- GAAAGAA-UGCGUGUAUUUUGUAA-3′) against human TRPM2 was designed using siDirect (Naito et al., 2004) and custom-made by Dharmacon. Control siRNA was from Ambion. OptiPrep was obtained from Sigma-Aldrich. The lysosome enrichment kit was from Thermo Scientific.

Antibodies and plasmids
For immunostaining, rat anti-HA (clone 3F10, Roche, 100 ng ml^{-1}), mouse anti-paxillin (cat no. 610569, BD Transduction Laboratories, 1:500), anti-CD63 (cat no. ab8219, Abcam, 1:500) and anti-c-Myc (cat no. 11667149001, Roche, 1:500) antibodies were used as primary antibodies. Alexa-Fluor-488-conjugated anti-rat-IgG (Life Technologies, 1:500) and Cy3-conjugated anti-mouse-IgG (Jackson ImmunoResearch, 1:500) were used as secondary antibodies. Mouse anti-LAMP1 (cat no. 611043, 1:5000)

and rabbit anti-calnexin (ab22595, 1:5000) antibodies were from BD Biosciences and Abcam, respectively. pActin-tdTomato and pLAMP1-GFP were kindly provided by Wolfgang Wagner (University Medical Center, Hamburg, Germany) and Patrice Boquet (Institut National de la Sante et la Recherché Medicale, Nice, France), respectively. Cdc42 (T17N and Q42L) and Rif (T17N and Q61L) constructs were kind gifts from Sreenivasan Ponnambalam (University of Leeds, Leeds, UK) and Harry Mellor (University of Bristol, Bristol, UK), respectively. siRNA-resistant TRPM2 cDNA in pcDNA3 was generated by introducing two silent mutations into the sequence at amino acid positions 71 (E) and 72 (C).

Cell culture and transfections
HeLa cells (ATCC CCl-185™) were maintained in Dulbecco's modified Eagle's medium (DMEM) with GlutaMAX-I supplemented with 10% fetal calf serum (FCS), penicillin (100 U/ml) and streptomycin (100 μg/ml). PC-3 cells (ATCC CRL-1435™) were cultured in RPMI-1640 with GlutaMAX™ medium supplemented with 10% heat-inactivated FCS, penicillin (100 U/ml), streptomycin (100 μg/ml), 1 mM sodium pyruvate, 50 μM 2-mercaptoethanol and 10 mM HEPES. Cells were cultured at 37°C under humidified 5% CO_2 and 95% air. Plasmid and siRNA transfections were performed using Lipofectamine 2000.

RT-PCR
RNA was extracted from HeLa and PC-3 cells using TRI-REAGENT. cDNA was synthesised from 5 μg of total RNA and subjected to PCR using TRPM2 primers: forward: 5′-ATGCTACCTCGGAAGCTGAA-3′ and reverse: 5′-TTCTGGAGGAGGGTCTTGTG-3′.

Isolation of lysosomes and western blotting
Lysosomes were isolated using an OptiPrep gradient centrifugation as described by Zhao et al. (2013). HeLa cells transfected with pcDNA-3-TRPM2-HA were homogenised using a ball-bearing homogeniser (Isobiotech, 16 micron clearance) and centrifuged at 500 g for 10 min to remove nuclei and cell debris. The supernatant was diluted with OptiPrep to 15% final concentration, overlaid on an OptiPrep step (17, 20, 23, 27, 30%) gradient and centrifuged in SW55 Ti rotor at 204,000 g for 4 h at 4°C. Lysosomes from the top fraction were collected, washed with PBS and analysed by western blotting.

Phalloidin staining of the actin cytoskeleton
Cells grown on coverslips to ∼50% confluence were treated with different drugs at 37°C for 2 h in standard buffered saline (SBS; 10 mM HEPES, 130 mM NaCl, 1.2 mM KCl, 8 mM glucose, 1.5 mM $CaCl_2$, 1.2 mM $MgCl_2$, pH 7.4) with or without H_2O_2 (see figure legends). Cells were fixed with 2% paraformaldehyde for 15 min, washed with phosphate-buffered saline (PBS), permeabilised with 0.2% Triton X-100 and 5% goat serum in PBS for 15 min and labelled with Alexa-Fluor-488- or Alexa-Fluor-666-conjugated phalloidin (1:1000 in goat serum). Images were collected with an LSM510 Meta confocal microscope using a 63×1.4 NA oil objective with an appropriate excitation and emission wavelengths.

Ca^{2+} and Zn^{2+} imaging
Cytosolic Ca^{2+} and Zn^{2+} levels were determined as described previously (Manna et al., 2015). Cells grown in 35 mm Fluorodish® glass-bottomed dishes were incubated at 37°C for 2 h with Fluo-4-AM (500 nM) or Fluozin-3-AM (1 μM) in SBS containing 0.01% Pluronic F127 with or without H_2O_2. After washing with SBS, cells were imaged with an LSM700 inverted confocal microscope using a 63×1.4 NA oil objective and excitation and emission wavelengths of 488 and 510 nm, respectively.

Immunostaining
Cells were fixed and permeabilised as above before incubation with an appropriate primary antibody at 37°C for 2 h. After three PBS washes, cells were labelled with relevant secondary antibodies, washed, mounted and imaged with an LSM510 Meta or Zeiss LSM 880 confocal microscope (equipped with an Airyscan superresolution imaging module) using a 63×1.4 NA oil objective and appropriate excitation (Alexa Fluor 488, 494 nm; Cy-3, 548 nm) and emission (Alexa Fluor 488, 519 nm; Cy-3, 562 nm) wavelengths.

Flow cytometry

Cells grown in a 24-well plate were treated with compounds as desired. Cytosolic Ca^{2+} and Zn^{2+} were labelled using Fluo-4-AM and FluoZin3-AM, respectively. Cells (>5000) were collected using trypsin-EDTA, washed and resuspended in SBS prior to analysis using a LSRFortessa™ flow cytometer (BD Biosciences).

Cell migration assay

Directional cell migration was examined by performing an agarose spot assay as described previously (Wiggins and Rappoport, 2010). Briefly, 90 µl of 0.5% molten low-melting-point agarose (Invitrogen) maintained at 40°C was mixed with 10 µl of 10× stock solutions of appropriate compounds to achieve the desired concentrations. A total of 10 µl of agarose was then spotted (four spots per plate) onto six-well plates (Greiner Bio One) and allowed to cool for 8 min at 4°C. Cells were then plated to ~60% confluence and allowed to adhere for 4 h before replacing with a medium containing 0.1% FCS. After 16 h at 37°C, images were collected using an EVOS®FL microscope fitted with a 10× objective (Life Technologies). Cells that appeared underneath the agarose spot were counted as migrated cells.

DCF-DA staining

Cells were stained for ROS using the 2′,7′-dichlorodihydrofluorescein diacetate (H2DCF-DA) reagent. After allowing HeLa cells to migrate into PBS- or H_2O_2-containing agarose spots for 6 h, cells were loaded with 10 µM H2DCF-DA for 30 min in Opti-Mem. After washing, fluorescence was imaged using an LSM700 inverted confocal microscope; excitation and emission wavelengths used were 488 nm and 519 nm, respectively.

Live-cell imaging of actin dynamics and lysosome migration into the agarose spot

Cells co-transfected with actin–Tdtomato and LAMP1–GFP plasmids were plated around the agarose spots in Fluorodish glass-bottomed dishes. After 16 h, cells at the boundary of the agarose spot were imaged with an LSM700 inverted confocal microscope using appropriate excitation (548 nm for actin–Tdtomato; 488 nm for LAMP1–GFP) and emission (562 nm for actin–Tdtomato; 519 nm for LAMP1–GFP) wavelengths and a 63×1.4NA oil objective.

Quantification of filopodia and focal adhesions

Quantification of filopodia was carried out as described previously (Bohil et al., 2006). Phalloidin-positive spike-like structures at cell periphery were counted as filopodia. A filopodium with branches was counted as one. Filopodia from five cells of an individual experiment were counted. The size $(0.1–1.0 \ \mu m^2)$ and number of focal adhesions were estimated from paxillin-stained cells using Image J.

Data analysis and presentation

All experiments were performed at least three times. Representative confocal images are presented. Fluorescence of cells was quantified using Image J (NIH). Data are presented as mean±s.e.m. Statistical significance was determined using a Student's t-test or one-way ANOVA with post-hoc Tukey test using Origin 8.6; a P-value of <0.05 was considered significant.

Author contributions

F.L. and N.A. performed the experiments and analysed data. A.S. and F.L. contributed to the conception and design of the experiments, interpretation of the data and preparation of the manuscript.

Supplementary information

Supplementary information available online at
http://jcs.biologists.org/lookup/suppl/doi:10.1242/jcs.179796/-/DC1

References

Bohil, A. B., Robertson, B. W. and Cheney, R. E. (2006). Myosin-X is a molecular motor that functions in filopodia formation. *Proc. Natl. Acad. Sci. USA* **103**, 12411-12416.

Brundage, R. A., Fogarty, K. E., Tuft, R. A. and Fay, F. S. (1991). Calcium gradients underlying polarization and chemotaxis of eosinophils. *Science* **254**, 703-706.

Chen, Y.-F., Chiu, W.-T., Chen, Y.-T., Lin, P.-Y., Huang, H.-J., Chou, C.-Y., Chang, H.-C., Tang, M.-J. and Shen, M.-R. (2011). Calcium store sensor stromal-interaction molecule 1-dependent signaling plays an important role in cervical cancer growth, migration, and angiogenesis. *Proc. Natl. Acad. Sci. USA* **108**, 15225-15230.

Dourdin, N., Bhatt, A. K., Dutt, P., Greer, P. A., Arthur, J. S. C., Elce, J. S. and Huttenlocher, A. (2001). Reduced cell migration and disruption of the actin cytoskeleton in calpain-deficient embryonic fibroblasts. *J. Biol. Chem.* **276**, 48382-48388.

Duncan, L. M., Deeds, J., Hunter, J., Shao, J., Holmgren, L. M., Woolf, E. A., Tepper, R. I. and Shyjan, A. W. (1998). Down-regulation of the novel gene melastatin correlates with potential for melanoma metastasis. *Cancer Res.* **58**, 1515-1520.

Eide, D. J. (2006). Zinc transporters and the cellular trafficking of zinc. *Biochim. Biophys. Acta* **1763**, 711-722.

Ellis, S. and Mellor, H. (2000). The novel Rho-family GTPase Rif regulates coordinated actin-based membrane rearrangements. *Curr. Biol.* **10**, 1387-1390.

Fabian, A., Fortmann, T., Dieterich, P., Riethmüller, C., Schön, P., Mally, S., Nilius, B. and Schwab, A. (2008). TRPC1 channels regulate directionality of migrating cells. *Pflügers Arch.* **457**, 475-484.

Fan, L., Pellegrin, S., Scott, A. and Mellor, H. (2010). The small GTPase Rif is an alternative trigger for the formation of actin stress fibers in epithelial cells. *J. Cell Sci.* **123**, 1247-1252.

Gardel, M. L., Schneider, I. C., Aratyn-Schaus, Y. and Waterman, C. M. (2010). Mechanical integration of actin and adhesion dynamics in cell migration. *Annu. Rev. Cell Dev. Biol.* **26**, 315-333.

Giannone, G., Dubin-Thaler, B. J., Rossier, O., Cai, Y., Chaga, O., Jiang, G., Beaver, W., Döbereiner, H.-G., Freund, Y., Borisy, G. et al. (2007). Lamellipodial actin mechanically links myosin activity with adhesion-site formation. *Cell* **128**, 561-575.

Gilbert, S. H., Perry, K. and Fay, F. S. (1994). Mediation of chemoattractant-induced changes in [Ca²⁺]i and cell shape, polarity, and locomotion by InsP3, DAG, and protein kinase C in newt eosinophils. *J. Cell Biol.* **127**, 489-503.

Giorgio, M., Trinei, M., Migliaccio, E. and Pelicci, P. G. (2007). Hydrogen peroxide: a metabolic by-product or a common mediator of ageing signals? *Nat. Rev. Mol. Cell Biol.* **8**, 722-728.

Hurd, T. R., DeGennaro, M. and Lehmann, R. (2012). Redox regulation of cell migration and adhesion. *Trends Cell Biol.* **22**, 107-115.

Johnson, H. W. and Schell, M. J. (2009). Neuronal IP3 3-kinase is an F-actin-bundling protein: role in dendritic targeting and regulation of spine morphology. *Mol. Biol. Cell* **20**, 5166-5180.

Klyubin, I. V., Kirpichnikova, K. M. and Gamaley, I. A. (1996). Hydrogen peroxide-induced chemotaxis of mouse peritoneal neutrophils. *Eur. J. Cell Biol.* **70**, 347-351.

Kukic, I., Kelleher, S. L. and Kiselyov, K. (2014). Zn²⁺ efflux through lysosomal exocytosis prevents Zn²⁺-induced toxicity. *J. Cell Sci.* **127**, 3094-3103.

Lamalice, L., Le Boeuf, F. and Huot, J. (2007). Endothelial cell migration during angiogenesis. *Circ. Res.* **100**, 782-794.

Lange, I., Yamamoto, S., Partida-Sanchez, S., Mori, Y., Fleig, A. and Penner, R. (2009). TRPM2 functions as a lysosomal Ca²⁺-release channel in β-Cells. *Sci. Signal.* **2**, ra23.

Manna, P. T., Munsey, T. S., Abuarab, N., Li, F., Asipu, A., Howell, G., Sedo, A., Yang, W., Naylor, J., Beech, D. J. et al. (2015). TRPM2-mediated intracellular Zn²⁺ release triggers pancreatic beta cell death. *Biochem. J.* **466**, 537-546.

Mathews, M. T. and Berk, B. C. (2008). PARP-1 inhibition prevents oxidative and nitrosative stress-induced endothelial cell death via transactivation of the VEGF receptor 2. *Arterioscler. Thromb. Vasc. Biol.* **28**, 711-717.

Mattila, P. K. and Lappalainen, P. (2008). Filopodia: molecular architecture and cellular functions. *Nat. Rev. Mol. Cell Biol.* **9**, 446-454.

Michels, J., Vitale, I., Saparbaev, M., Castedo, M. and Kroemer, G. (2014). Predictive biomarkers for cancer therapy with PARP inhibitors. *Oncogene* **33**, 3894-3907.

Monet, M., Lehen'kyi, V., Gackiere, F., Firlej, V., Vandenberghe, M., Roudbaraki, M., Gkika, D., Pourtier, A., Bidaux, G., Slomianny, C. et al. (2010). Role of cationic channel TRPV2 in promoting prostate cancer migration and progression to androgen resistance. *Cancer Res.* **70**, 1225-1235.

Naito, Y., Yamada, T., Ui-Tei, K., Morishita, S. and Saigo, K. (2004). siDirect: highly effective, target-specific siRNA design software for mammalian RNA interference. *Nucleic Acids Res.* **32**, W124-W129.

Niethammer, P., Grabher, C., Look, A. T. and Mitchison, T. J. (2009). A tissue-scale gradient of hydrogen peroxide mediates rapid wound detection in zebrafish. *Nature* **459**, 996-999.

Nilius, B. and Szallasi, A. (2014). Transient receptor potential channels as drug targets: from the science of basic research to the art of medicine. *Pharmacol. Rev.* **66**, 676-814.

Nobes, C. D. and Hall, A. (1995). Rho, rac, and cdc42 GTPases regulate the assembly of multimolecular focal complexes associated with actin stress fibers, lamellipodia, and filopodia. *Cell* **81**, 53-62.

Polytarchou, C., Hatziapostolou, M. and Papadimitriou, E. (2005). Hydrogen peroxide stimulates proliferation and migration of human prostate cancer cells through activation of activator protein-1 and up-regulation of the heparin affin regulatory peptide gene. *J. Biol. Chem.* **280**, 40428-40435.

Potier, M., Gonzalez, J. C., Motiani, R. K., Abdullaev, I. F., Bisaillon, J. M., Singer, H. A. and Trebak, M. (2009). Evidence for STIM1- and Orai1-dependent store-operated calcium influx through ICRAC in vascular smooth muscle cells: role in proliferation and migration. *FASEB J.* **23**, 2425-2437.

Prevarskaya, N., Skryma, R. and Shuba, Y. (2011). Calcium in tumour metastasis: new roles for known actors. *Nat. Rev. Cancer* **11**, 609-618.

Ridley, A. J. (2001). Rho GTPases and cell migration. *J. Cell Sci.* **114**, 2713-2722.

Ridley, A. J. and Hall, A. (1992). The small GTP-binding protein rho regulates the assembly of focal adhesions and actin stress fibers in response to growth factors. *Cell* **70**, 389-399.

Ridley, A. J., Schwartz, M. A., Burridge, K., Firtel, R. A., Ginsberg, M. H., Borisy, G., Parsons, J. T. and Horwitz, A. R. (2003). Cell migration: integrating signals from front to back. *Science* **302**, 1704-1709.

Sensi, S. L., Paoletti, P., Bush, A. I. and Sekler, I. (2009). Zinc in the physiology and pathology of the CNS. *Nat. Rev. Neurosci.* **10**, 780-791.

Sigal, Y. J., Quintero, O. A., Cheney, R. E. and Morris, A. J. (2007). Cdc42 and ARP2/3-independent regulation of filopodia by an integral membrane lipid-phosphatase-related protein. *J. Cell Sci.* **120**, 340-352.

Small, J. V., Stradal, T., Vignal, E. and Rottner, K. (2002). The lamellipodium: where motility begins. *Trends Cell Biol.* **12**, 112-120.

Somlyo, A. V., Bradshaw, D., Ramos, S., Murphy, C., Myers, C. E. and Somlyo, A. P. (2000). Rho-kinase inhibitor retards migration and in vivo dissemination of human prostate cancer cells. *Biochem. Biophys. Res. Commun.* **269**, 652-659.

Sumoza-Toledo, A. and Penner, R. (2011). TRPM2: a multifunctional ion channel for calcium signalling. *J. Physiol.* **589**, 1515-1525.

Sumoza-Toledo, A., Lange, I., Cortado, H., Bhagat, H., Mori, Y., Fleig, A., Penner, R. and Partida-Sánchez, S. (2011). Dendritic cell maturation and chemotaxis is regulated by TRPM2-mediated lysosomal Ca^{2+} release. *FASEB J.* **25**, 3529-3542.

Takahashi, N., Kozai, D., Kobayashi, R., Ebert, M. and Mori, Y. (2011). Roles of TRPM2 in oxidative stress. *Cell Calcium* **50**, 279-287.

Takatani-Nakase, T., Matsui, C., Maeda, S., Kawahara, S. and Takahashi, K. (2014). High glucose level promotes migration behavior of breast cancer cells through zinc and its transporters. *PLoS ONE* **9**, e90136.

Tian, D., Jacobo, S. M. P., Billing, D., Rozkalne, A., Gage, S. D., Anagnostou, T., Pavenstädt, H., Hsu, H.-H., Schlondorff, J., Ramos, A. and Greka, A. (2010). Antagonistic regulation of actin dynamics and cell motility by TRPC5 and TRPC6 channels. *Sci. Signal.* **3**, ra77.

Tojkander, S., Gateva, G. and Lappalainen, P. (2012). Actin stress fibers - assembly, dynamics and biological roles. *J. Cell Sci.* **125**, 1855-1864.

Tsai, F.-C., Seki, A., Yang, H. W., Hayer, A., Carrasco, S., Malmersjö, S. and Meyer, T. (2014). A polarized Ca^{2+}, diacylglycerol and STIM1 signalling system regulates directed cell migration. *Nat. Cell Biol.* **16**, 133-144.

Turner, C. E. (2000). Paxillin and focal adhesion signalling. *Nat. Cell Biol.* **2**, E231-E236.

Vicente-Manzanares, M., Ma, X., Adelstein, R. S. and Horwitz, A. R. (2009). Non-muscle myosin II takes centre stage in cell adhesion and migration. *Nat. Rev. Mol. Cell Biol.* **10**, 778-790.

Waning, J., Vriens, J., Owsianik, G., Stüwe, L., Mally, S., Fabian, A., Frippiat, C., Nilius, B. and Schwab, A. (2007). A novel function of capsaicin-sensitive TRPV1 channels: involvement in cell migration. *Cell Calcium* **42**, 17-25.

Wei, C., Wang, X., Chen, M., Ouyang, K., Song, L.-S. and Cheng, H. (2009). Calcium flickers steer cell migration. *Nature* **457**, 901-905.

Wei, C., Wang, X., Zheng, M. and Cheng, H. (2012). Calcium gradients underlying cell migration. *Curr. Opin. Cell Biol.* **24**, 254-261.

Wiggins, H. and Rappoport, J. (2010). An agarose spot assay for chemotactic invasion. *Biotechniques* **48**, 121-124.

Wondergem, R., Ecay, T. W., Mahieu, F., Owsianik, G. and Nilius, B. (2008). HGF/SF and menthol increase human glioblastoma cell calcium and migration. *Biochem. Biophys. Res. Commun.* **372**, 210-215.

Yang, S., Zhang, J. J. and Huang, X.-Y. (2009a). Orai1 and STIM1 are critical for breast tumor cell migration and metastasis. *Cancer Cell* **15**, 124-134.

Yang, Z.-H., Wang, X.-H., Wang, H.-P. and Hu, L.-Q. (2009b). Effects of TRPM8 on the proliferation and motility of prostate cancer PC-3 cells. *Asian J. Androl.* **11**, 157-165.

Yang, W., Manna, P. T., Zou, J., Luo, J., Beech, D. J., Sivaprasadarao, A. and Jiang, L.-H. (2011). Zinc inactivates melastatin transient receptor potential 2 channels via the outer pore. *J. Biol. Chem.* **286**, 23789-23798.

Yoo, S. K., Starnes, T. W., Deng, Q. and Huttenlocher, A. (2011). Lyn is a redox sensor that mediates leukocyte wound attraction in vivo. *Nature* **480**, 109-112.

Zeng, Z., Inoue, K., Sun, H., Leng, T., Feng, X., Zhu, L. and Xiong, Z.-G. (2015). TRPM7 regulates vascular endothelial cell adhesion and tube formation. *Am. J. Physiol. Cell Physiol.* **308**, C308-C318.

Zhao, H., Ruberu, K., Li, H. and Garner, B. (2013). Analysis of subcellular [57Co] cobalamin distribution in SH-SY5Y neurons and brain tissue. *J. Neurosci. Methods* **217**, 67-74.